GRB 090423 at a redshift of $z \simeq 8.1$

R. Salvaterra [1], M. Della Valle [2] [3] [4], S. Campana [1], G. Chincarini [5] [1], S. Covino [1], P. D'Avanzo [5] [1], A. Fernández-Soto [6], C. Guidorzi [7], F. Mannucci [8], R. Margutti [5] [1], C.C. Thöne [1], L.A. Antonelli [9], S.D. Barthelmy [10], M. De Pasquale [11], V. D'Elia [9], F. Fiore [9], D. Fugazza [1], L.K. Hunt [8], E. Maiorano [12], S. Marinoni [13] [14], F.E. Marshall [10], E. Molinari [13] [1] J. Nousek [15], E. Pian [16] [17], J.L. Racusin [15], L. Stella [9], L. Amati [12], G. Andreuzzi [13], G. Cusumano [18], E.E. Fenimore [19], P. Ferrero [20], P. Giommi [21], D. Guetta [9], S.T. Holland [10] [22] [23], K. Hurley [24], G.L. Israel [9], J. Mao [1], C.B. Markwardt [10] [23] [25], N. Masetti [12], C. Pagani [15], E. Palazzi [12], D.M. Palmer [18], S. Piranomonte [9], G. Tagliaferri [1], V. Testa [9]

[1] INAF, Osservatorio Astronomico di Brera, via E. Bianchi 46, I-23807 Merate (LC), Italy
[2] INAF, Osservatorio Astronomico di Capodimonte, Salita Moiariello 16, 80131 Napoli, Italy
[3] European Southern Observatory (ESO), 85748 Garching, Germany
[4] International Centre for Relativistic Astrophysics, Piazzale della Repubblica 2, 65122 Pescara, Italy
[5] Dipartimento di Fisica G. Occhialini, Università di Milano Bicocca, Piazza della Scienza 3, I-20126 Milano, Italy
[6] Instituto de Fisica de Cantabria, CSIC-Univ. Cantabria, Av. de los Castros s/n, E-39005 Santander, Spain
[7] Dipartimento di Fisica, Universita' di Ferrara, via Saragat 1, I-44100 Ferrara, Italy
[8] INAF, Osservatorio Astrofisico di Arcetri, Largo E. Fermi 5, I-50125 Firenze, Italy
[9] INAF, Osservatorio Astronomico di Roma, Via di Frascati 33, I-00040, Monte Porzio Catone, Rome, Italy
[10] NASA,Goddard Space Flight Center, Greenbelt, MD 20771, USA
[11] Mullard Space Science Laboratory (UCL), Holmbury Rd, Holmbury St.Mary, Dorking, RH5 6NT, UK
[12] INAF, IASF di Bologna, via Gobetti 101, I-40129 Bologna, Italy
[13] INAF, Fundación Galileo Galilei, Rambla José Ana Fernández Pérez, 7 38712 Breña Baja, TF - Spain
[14] Universitá degli Studi di Bologna, via Ranzani, 1, Bologna, Italy
[15] Department of Astronomy and Astrophysics, Pennsylvania State University, University Park, PA 16802, USA
[16] INAF, Trieste Astronomical Observatory, Via G.B. Tiepolo 11, I-34143 Trieste, Italy
[17] Scuola Normale Superiore, Piazza dei Cavalieri 1, 56100 Pisa, Italy
[18] INAF, Istituto di Astrofisica Spaziale e Fisica Cosmica di Palermo, Via Ugo La Malfa 153, 90146 Palermo, Italy
[19] Los Alamos National Laboratory, P.O. Box 1663, Los Alamos, NM, 87545, USA
[20] Thüringer Landessternwarte Tautenburg, Sternwarte 5, D-07778, Tautenburg, Germany
[21] ASI Science Data Center, ASDC c/o ESRIN, via G. Galilei, 00044 Frascati, Italy
[22] Universities Space Research Association, 10211 Wincopin Circle, Suite 500, Columbia, MD, 21044, USA
[23] Centre for Research and Exploration in Space Science and Technology, Code 668.8, Greenbelt, MD, 20771, USA
[24] Space Sciences Laboratory, 7 Gauss Way, University of California, Berkeley, CA 94720-7450, USA
[25] Department of Astronomy, University of Maryland, College Park, MD 20742, USA

Gamma-ray bursts (GRBSs) are produced by rare types of massive stellar explosions. Their rapidly fading afterglows are often bright enough at optical wavelengths, that they are detectable up to cosmological distances. Hirtheto, the highest known redshift for a GRB was $z = 6.7$ (ref. 1), for GRB 080913, and for a galaxy was $z = 6.96$ (ref. 2). Here we

report observations of GRB 090423 and the near-infrared spectroscopic measurement of its redshift $z = 8.1^{+0.1}_{-0.3}$. This burst happened when the Universe was only $\sim 4\%$ of its current age[3]. Its properties are similar to those of GRBs observed at low/intermediate redshifts, suggesting that the mechanisms and progenitors that gave rise to this burst about 600 million years after the Big Bang are not markedly different from those producing GRBs ~ 10 billion years later.

GRB 090423 was detected by NASA's Swift satellite on 23 April 2009 at 07:55:19 UT as a double-peaked burst of duration $T_{90} = 10.3 \pm 1.1$ s. As observed by Swift's Burst Alert Telescope (BAT)[4], it had a 15–150 keV fluence $F = (5.9 \pm 0.4) \times 10^{-7}$ erg cm^{-2} and a peak energy $E_p = 48^{+6}_{-5}$ keV (errors at 90% confidence level). Its X-ray afterglow was identified by Swift's X-ray Telescope (XRT), which began observations 73 s after the BAT trigger[5]. A prominent flare was detected at $t \sim 170$ s in the X-ray light curve, which shows that a typical 'steep decay/plateau/normal decay' behaviour (Fig. 1). Swift's UltraViolet Optical Telescope (UVOT) did not detect a counterpart even though it started settled explosures only 77 s after the trigger[6]. A 2μm counterpart was detected with the United Kingdom Infra-Red Telescope (UKIRT, Hawaii) 20 min after the trigger[7]. Evidence that this burst occurred at high redshift, was given by the multi-band imager Gamma-Ray Burst Optical/Near-Infrared Detector (GROND, Chile) multiband imager (from g' band to K band), which indicated a photometric redshift of $z = 8.0^{+0.4}_{-0.8}$ (ref. 7).

We used the 3.6m Telescopio Nazionale Galileo (TNG, La Palma) with the Near Infrared Camera Spectrometer (NICS) and the Amici prism to obtain a low-resolution ($R \approx 50$) spectrum of GRB 090423 ~ 14 hrs after the trigger. NICS/Amici is an ideal instrument to detect spectral breaks in the continuum of faint objects because of its high efficiency and wide simultaneous spectral coverage (0.8-2.4 μm). The spectrum (Fig. 2) reveals a clear break at a wavelength of 1.1 μm (ref. 8). We derive a spectroscopic redshift for the GRB of $z = 8.1^{+0.1}_{-0.3}$ (ref. 9; see Supplementary Information, section 3), interpreting the break as Lyman-α absorption in the intergalactic medium. No other significant absorption features were detected. This result is consistent, within the errors, with the measurement reported in ref. 7.

At $z \sim 8.1$, GRB 090423 has a prompt-emission rest-frame duration of only $T_{90,rf} = 1.13 \pm 0.12$ s in the redshifted 15-150 keV energy band, an isotropic equivalent energy $E_{iso} = 1.0 \pm 0.3 \times 10^{53}$ erg in the redshifted 8-1000 keV energy band[10] and a peak energy $E_{p,rf} = 437 \pm 55$ keV. The short duration and

the high peak energy are consistent both with the distribution of long bursts, linked to massive stellar collapse, and with the population of short bursts, thought to arise from the merger of binary compact stars[11,12]. Although the analysis of the spectral lag between the high- and low-energy channels in the BAT band is inconclusive about the classification of GRB 090423, the high E_{iso} argues in favor of a long GRB. The fact that GRB 090423 matches the $E_{iso} - E_{p,rf}$ correlation of long GRBs within 0.5σ further supports this classification[33] (Supplementary Fig. 2).

The rest-frame $\gamma-$ray and X-ray light curve of GRB 090423 is remarkably akin to those of long GRBs at low, intermediate and high redshifts (Fig. 1), suggesting similar physics and interaction with the circumburst medium. The near-infrared light curve of GRB 090423 $\sim$ 15h after the trigger shows a temporal decay with a power-law index of $\alpha_0 \sim 0.5$, which is markedly different from the decay observed at X-ray energies during the same time interval, which has a power-law index of $\alpha_{X,2} \sim 1.3$ (Supplementary Fig. 3 and Supplementary Information, section 2). As for other lower-redshift GRBs, this behaviour is difficult to reconcile with standard afterglow models, although the sampling of the near-infrared light curve is too sparse for any firm conclusion to be drawn.

The spectral energy distribution of near-infrared afterglow is well fitted by a power-law with an index of $\beta = 0.4^{+0.2}_{-1.4}$ and an equivalent interstella extinction of E$(B - V)<$ 0.15, assuming dust reddening consistent with the Small Magellanic Cloud[9]. On the other hand, the analysis of the XRT data in the time interval 3900s–21568s suggests the presence of intrinsic absorption (in excess of the Galactic value) with an equivalent hydrogen column density of $N_H(z) = 6.8^{+5.6}_{-5.3} \times 10^{22}$ cm^{-2} (90% confidence level; Supplementary Information, section 1). The low value of the dust extinction coupled with a relatively high value of N_H suggests that GRB 090423 originates from a region with low dust content relative to those of low-z GRBs[14], but one similar to that of the high-z GRB 050904, for which $z = 6.3$ (ref. 15). Because the absorbing medium must be thin from the point of view of "Thomson" scattering, the metallicity of the circumburst medium can be constrained to be $> 4\%$ of the solar value, $Z_\odot$. The implication is that previous supernova explosions have already enriched the host galaxy of GRB 090423 to more than the critical metallicity, $Z \sim 10^{-4}$ $Z_\odot$ (ref. 16) that prevents the formation of very massive stars (population III stars). Therefore the progenitor of GRB 090423 should belong to a second stellar generation. Its explosion injected fresh metals into the interstellar medium, further contributing to the enrichment of its host galaxy. Its existence empirically supports the cosmological models[17,18] in which stars and galaxies, already enriched by metals, are in place only $\sim$ 600 million years after the Big Bang. Long GRBs are mostly associated with star forming dwarf galaxies, which are thought to be the

dominant population of galaxies in the early Universe[19]. The fact that GRB 090423 appears to have exploded in an environment similar to that of low-z GRB hosts[20] is in agreement with this.

The occurrence of a GRB at $z \sim 8$ has important implications for the cosmic history of these objects[21,22,23,24]. In a first, simple approach, we can assume that GRBs trace the cosmic star formation history, given the well-known link of the long GRBs and the deaths of massive stars[25], and that GRBs are well described by a universal luminosity function. However, under these assumptions the expected number of bursts at $z \geq 8$ with an observed photon peak flux larger than or equal to that of GRB 090423 is extremely low: $\sim 4 \times 10^{-4}$ in ~ 4 yrs of Swift operation (Supplementary Fig. 6 and Supplementary Information, section 4). Hence, one or both of the above assumptions may be oversimplification[24,26]. The detection of a very high-z burst such as GRB 090423 could be accomodated if the GRB luminosity function were shifted towards higher luminosity according to $(1 + z)^{\delta}$ with $\delta \gtrsim 1.5$ or if the GRB formation rate were strongly enhanced in galaxies with $Z \lesssim 0.2Z_{\odot}$. The requirement for evolution may be mitigate if we assume a very high star formation rate at $z > 8$. However, we note that the need for evolution is strongly supported by both the large number of Swift detections at $z > 2.5$ (ref. 24) and the number of bursts with peak luminosities in excess of 10^{53} erg s^{-1} (ref. 26). A possible explanation is that high-redshift galaxies are characterized by a top-heavy (bottom-light) stellar initial mass function with a higher incidence of massive stars than in the local Universe[27], providing an enhanced number of GRB progenitors. Such objects could be the main agents responsible for completing the reionization of the Universe[28,19,29,30].

1. Greiner, J. *et al.* GRB 080913 at redshift 6.7. *Astrophys. J.* **693**, 1610-1620 (2009).

2. Iye, M. *et al.* A galaxy at a redshift $z = 6.96$. *Nature* **443**, 186-188 (2006)

3. Komatsu, E. *et al.*, Five-Year Wilkinson Microwave Anisotropy Probe Observations: Cosmological Interpretation. *Astrophys. J. Suppl. Ser.* **180**, 330-376 (2009).

4. Palmer, D.M. *et al.* GRB 090423: Swift-BAT refined analysis. *GCN Circ.* 9204 (2009).

5. Stratta, G. & Perri, M. GRB 090423: Swift-XRT refined analysis. *GCN Circ.* 9212 (2009).

6. De Pasquale, M. & Krimm, H. GRB090423 - Swift/UVOT upper limits. *GCN Circ.* 9210 (2009).

7. Tanvir, N. *et al.*, A glimpse of the end of the dark ages: the γ-ray burst of 23 April 2009 at redshift 8.3. *Nature* submitted (2009).

8. Thoene, C.C. *et al.* GRB 090423: TNG Amici spectrum. *GCN Circ.* 9216 (2009).

9. Fernández-Soto, A. *et al.* GRB 090423: Refined TNG analysis. *GCN Circ.* 9222 (2009).

10. von Kienlin, A. GRB 090423: Fermi GBM observation. *GCN Circ.* 9229 (2009).

11. Mészáros, P. Gamma-ray bursts. *Rep. Prog. Phys.* **69**, 2259-2322 (2006).

12. Zhang, B. Gamma-Ray Bursts in the Swift Era. *Chin. J. Astron. Astrophys.* **7**, 1-50 (2007).

13. Amati, L. *et al.* On the consistency of peculiar GRBs 060218 and 060614 with the $E_{p,i} - E_{iso}$ correlation. *Astron. Astrophys.* **463**, 913-919 (2007).

14. Schady, P. *et al.* Dust and gas in the local environments of gamma-ray bursts. *Mon. Not. R. Astron. Soc.* **377**, 273-284 (2007)

15. Stratta, G. *et al.* Dust Properties at $z = 6.3$ in the Host Galaxy of GRB 050904. *Astrophys. J. Lett.* **661**, 9-12 (2007).

16. Schneider, R. *et al.* First Stars, Very Massive Black Holes, and Metals. *Astrophys. J.* **571**, 30-39 (2002).

17. Springel, V. *et al.* Simulations of the formation, evolution and clustering of galaxies and quasars. *Nature* **435**, 629-636 (2005).

18. Nagamine, K. *et al.* Tracing early structure formation with massive starburst galaxies and their implications for reionization. *New Astron.* **50**, 29-34 (2006).

19. Choudhury, T.R., Ferrara, A., Gallerani, S. On the minimum mass of reionization sources. *Mon. Not. R. Astron. Soc.* **385** L58-L62 (2008).

20. Fruchter, A.S. *et al.* Long γ-ray bursts and core-collapse supernovae have different environments. *Nature* **7092**, 463-468 (2006).

21. Lamb, D.Q., & Reichart, D.E. Gamma-Ray Bursts as a Probe of the Very High Redshift Universe. *Astrophys. J.* **536**, 1-18 (2000).

22. Guetta, D., Piran, T., Waxman, E. The Luminosity and Angular Distributions of Long-Duration Gamma-Ray Bursts. *Astrophys. J.* **619**, 412-419 (2005)

23. Bromm, V. & Loeb, A. High-Redshift Gamma-Ray Bursts from Population III Progenitors. *Astrophys. J.* **642**, 382-388 (2006).

24. Salvaterra, R. & Chincarini, G. The Gamma-Ray Burst Luminosity Function in the light of the Swift 2 year data. *Astrophys. J. Lett.* **656**, 49-52 (2007).

25. Woosley, S. E. & Bloom, J. S. The Supernova Gamma-Ray Burst Connection. *Annu. Rev. Astron. Astrophys.* **44**, 507-556 (2006).

26. Salvaterra, R. *et al.* Evidence for Luminosity Evolution of Long Gamma-ray Bursts in Swift Data. *Mon. Not. R. Astron. Soc.* **396**, 299-303 (2009).

27. Chary, R.-R. The Stellar Initial Mass Function at the Epoch of Reionization. *Astrophys. J.* **680**, 32-40 (2008).

28. Bolton, J.S. & Haehnelt, M.G. The observed ionization rate of the intergalactic medium and the ionizing emissivity at $z \geq 5$: evidence for a photon-starved and extended epoch of reionization. *Mon. Not. R. Astron. Soc.* **382**, 325-341 (2007).

29. Furlanetto, S.R. & Mesinger, A. The ionizing background at the end of reionization. *Mon. Not. R. Astron. Soc.* **394**, 1667-1673 (2009).

30. Stiavelli, M. *From First Light to Reionization: The End of the Dark Ages.* Vch Verlagsgesellschaft Mbh. (2009).
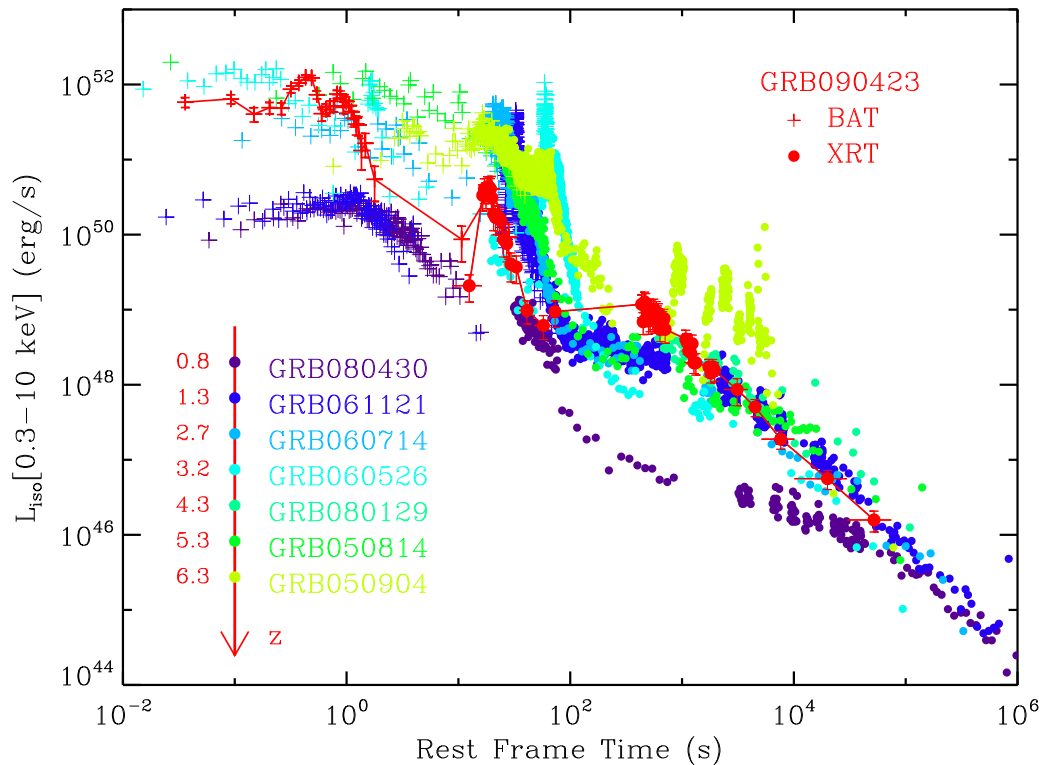
Figure 1. Rest-frame γ-ray and X-ray light curves for bursts at different redshifts. BAT and XRT light curve of GRB 090423 (red data) in the source rest-frame. Errors on luminosity, L_{iso}, are at 1σ level; horizontal bars refer to the integration time interval. The XRT 0.3–10 keV light-curve shows a prominent flare at a rest-frame time of $t_{rf} \sim 18$ s (also detected by BAT), and a flat phase (with a power-law index of $\alpha_{X,1} = 0.13 \pm 0.11$) followed by a rather typical decay with power-law index $\alpha_{X,2} = 1.3 \pm 0.1$. We compare the light curve of GRB 090423 with those of seven GRBs in the redshift interval 0.8-6.3. The bursts are selected from among those showing a canonical three-phase behaviour (steep decay/plateau/normal decay) in the X-ray light curve and without a spectral break between BAT and XRT, allowing the spectral calibration of the BAT signal into the 0.3-10 keV energy band. The light curve of GRB 090423 does not show any distinguishing features relative to those of the lower-redshift bursts, suggesting that the physical mechanism that causes the GRB and its interaction with the circumburst medium are similar at $z \sim 8.1$ and at lower redshifts.
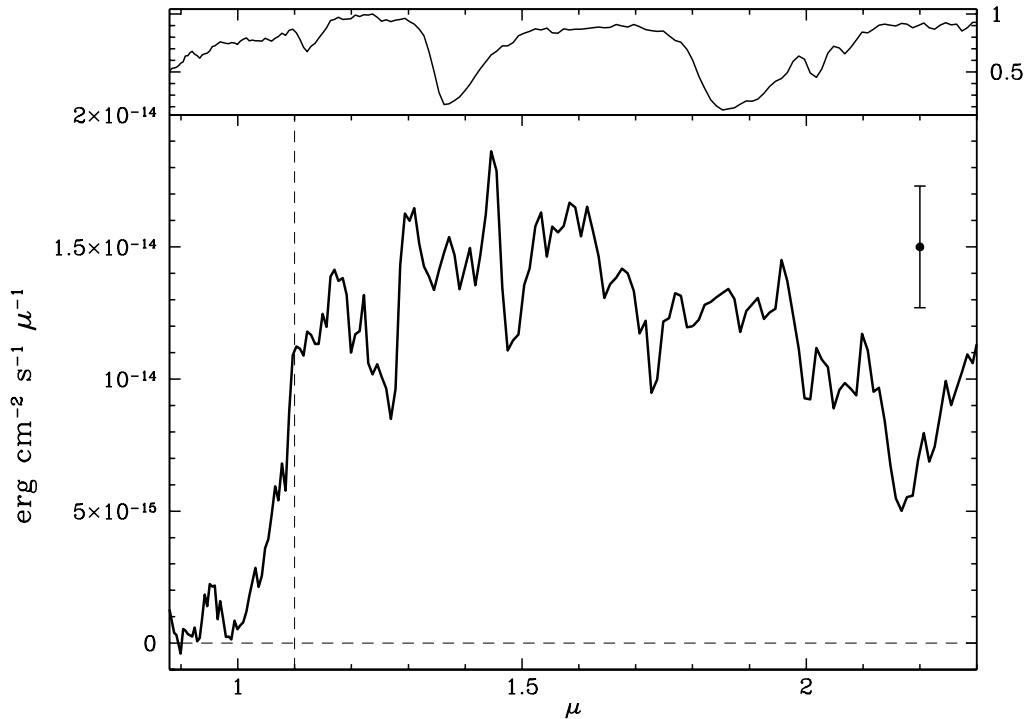
Figure 2. TNG spectrum of the NIR afterglow. Bottom Panel. Spectrum of GRB 090423 obtained using the Amici prism on the Telescopio Nazionale Galileo (TNG). The sharp break at wavelength $\lambda \approx 1.1$ μm, which is due to the HI absorption in the intergalactic medium at the wavelength of the Lyα line, implies that $z = 8.1^{+0.1}_{-0.3}$. The spectrum has been smoothed with a boxcar filter of width $\Delta = 25$ pixels (where one pixel corresponds to ~ 0.006 μm at $\lambda = 1.1\mu$m). The absolute flux calibration was obtained by matching the almost simultaneous GROND photometric measurements[7]. The wavelength calibration was obtained from the TNG archive and adjusted to the wavelengths of the main atmospheric bands. The error bar corresponds to $\pm 1\sigma$ uncertainty as measured on the smoothed spectrum. The confidence level of the Lyman-α break detection is $\gtrsim 4\sigma$. See also Supplementary Information, section 3. Top Panel. Plot of the trasmittance (the atmospheric transparency convolved with the instrumental response). The system has a significant sensitivity down to 0.9 μm, and no instrumental or atmospheric effect could explain the abrupt flux break observed in the spectrum of GRB 090423.

Supplementary Information

This material presents technical details to support the discussion in the main paper. We discuss here the Swift data analysis, the analysis of the photometric data, the details of the analysis of the TNG spectroscopic data and the modelling of the GRB redshift distribution.

1. Swift data analysis

Swift-BAT triggered on GRB 090423 at 07:55:19.35 UT on 23 April 2009. BAT data were analysed using the HEASOFT software package (version 6.6.2) with the Swift Calibration Database (CALDB) version BAT(20090130). Background-subtracted light curves in different energy channels, energy spectra and corresponding response functions were derived from the BAT event file as processed with the BAT software tool `batgrbproduct`, by using the mask-weighting technique for the BAT refined position[4], and by using standard and BAT-dedicated software tools. The mask-weighted light curve (Supplementary Figure 1) showed a couple of overlapping peaks starting at $T_0 - 2$ s, peaking at $T_0 + 4$ s, and ending at $T_0 + 15$ s. The estimated duration, T_{90}, was 10.3 ± 1.1 s for the mask-weighted light curve in the 15-150 keV band. T_{90} is defined as the duration 90% of the total prompt γ-ray fluence in the observer frame (i.e. the interval from 5% to 95% of the total fluence) and is estimated using the `battblocks` software tool. Noteworthy is the light curve of the hardest channel, from 100 to 150 keV, showing a very weak signal as compared with those of the other energy channels. This reflects the spectral softness of this GRB, as shown also by the total energy spectrum. The latter was accumulated from -0.7 to 11.7 s and is fitted with a cut-off power law, $N(E) \sim E^{-\Gamma} \exp[(2 - \Gamma)E/E_p]$, with the best-fit value for the peak energy, $E_p = 48^{+6}_{-5}$ keV, and a photon index $\Gamma = 0.6^{+0.5}_{-0.6}$. This value of E_p is fully consistent with that determined by fitting the Fermi/Gamma-ray Burst Monitor spectrum[10] with the canonical "Band" function[31]. The corresponding total fluence in the 15-150 keV energy band is $(5.9 \pm 0.4) \times 10^{-7}$ erg cm^{-2}. The 1-s peak photon flux measured from 3.5 s in the 15-150 keV band is 1.7 ± 0.2 ph s^{-1} cm^{-2}. Uncertainties are given at 90% confidence. At $z = 8.1$, GRB 090423 is found to be consistent with the $E_{\mathrm{p,rf}} - E_{iso}$ correlation[13] within 0.5σ (Supplementary Figure 2). We note that, even considering the measured peak energy as obtained by a fit of the Fermi/GBM data with a cut-off power-law spectrum, i.e. $E_p = 82 \pm 15$ keV and thus $E_{p,rf} = 746 \pm 137$ keV (ref. [10]), GRB 090423 would still be consistent within 2σ with the $E_{p,rf} - E_{iso}$ correlation.

The BAT light curve shown in Supplementary Figure 3 is the mask-weighted curve extracted between

15 and 150 keV, binned so as to ensure S/N> 2 with a minimum binning time of 0.512 s. Extrapolation of the BAT flux down to the 0.3-10 keV band was performed by assuming the above spectral model. We note that the remarkable X-ray flare detected by XRT is seen in the BAT data as well. We note that assuming that the flare is still part of the prompt emission[32], the total duration of the prompt phase in the source rest frame might be $\sim$ 20s, similar to other long GRBs.

The XRT observations began 73 s after the trigger: up to $\sim$ 300 s the signal was dominated by a flare. As in many other GRBs, the light-curve then flattened to a shallow decay phase which could be well modelled by a power-law with index $\alpha_{X,1} = 0.13 \pm 0.11$. At $t \sim 4500$ s the X-ray afterglow steepened to $\alpha_{X,2} = 1.3 \pm 0.1$ (errors at 68% confidence level). The flare was modelled by a standard profile[34]: this is characterised by a $1/e$ rise-time $t_{rise} = 29.1 \pm 3.6$ s; $1/e$ decay-time $t_{decay} = 65.5 \pm 3.6$ s; $1/e$ width of $\Delta t = 94.6 \pm 7.3$ s, while the asymmetry parameter is $k = 0.38 \pm 0.03$. This implies a variability measure $\Delta t/t_{peak} = 0.66$ and a brightness contrast ΔFlux/Flux around 25. While the flare parameters are defined following ref. [34], the reported uncertainties are worked out by using the entire covariance matrix. At the redshift of the burst, the flare has an energy $E_{iso} = 3.6 \times 10^{51}$ erg in the redshifted 0.3-10 keV band of XRT, comparable to the energy released during the prompt emission of other GRBs.

To evaluate the intrinsic column density absorbing the GRB 090423 spectrum, we extracted data in the 3900–21568 s time interval (observer frame). This interval was selected in order to avoid the bright X-ray flare whose variable spectrum might alter the fit and in order to have sufficient signal in the extraction region which we define as a count rate of more than 0.01 counts s^{-1}. The resulting 7984 s exposure contains 680 counts in the range between 0.3-10 keV. The ancillary response file (arf) was created with the task `xrtmkarf` (within `heasoft` v.6.2.2) using the relevant exposure file and the latest v.11 reponse matrix function (rmf). The spectrum was binned to 20 counts per bin in order to assure a reasonable χ^2 statistic.

We fit the X-ray spectrum with a composite absorption model consisting of a Galactic contribution and an intrinsic absorption fixed to z=8.1 using the `tbabs` model within the XSPEC (v12.5.0aa) package. We left the Galactic value free to vary in the $2.9 - 3.2 \times 10^{20}$ cm^{-2} range (based on the absorption maps by [35] and [36]). The X-ray continuum was modeled with a power law, as is customary for the afterglow spectra of GRBs. The overall fit is good with a reduced $\chi^2_{\rm red} = 1.12$ (28 degrees of freedom, corresponding to a null hypothesis probability of 30%). The resulting power law photon index is $\Gamma_X = 1.97^{+0.15}_{-0.16}$.

For the intrinsic column density, we get a value of $N_H(z) = 6.8^{+5.6}_{-5.3} \times 10^{22}$ cm^{-2} (90% confidence level), among the highest of all Swift GRBs[37]. The results refer to a solar composition and metallicity. Assuming that the medium is not Thomson thick, a lower limit of the metallicity can be obtained by $N_H(z) \lesssim (1/\sigma_T)(Z/Z_\odot)^{-1}$, where σ_T is the Thomson cross-section (e.g. ref. [38]). We find $Z > 0.043 \, Z_\odot$. A lower limit on the value of $N_H(z) > 6 \times 10^{21}$ cm^{-2} is found at 95% confidence level corresponding to a lower limit on the metallicity of $Z > 0.004 \, Z_\odot$.

2. Analysis of the photometric data

We analyzed all the available photometric data[7] by using the /it zphrem code**??**, in order to determine the photometric redshift and spectral properties of the afterglow. Our code fits a model of functional form $f_\nu \propto \nu^{-\beta} t^{-\alpha_O}$, including dust extinction (by an SMC-type extinction law) as a free parameter.

We find that the data are best fit within the time range $4.2 \times 103 < t < 6.6 \times 104$ s) with a model characterised by a temporal decay with a power law index $\alpha_O = 0.50 \pm 0.05$ (we quote hereafter 95% confidence intervals). The dust content is constrained to be $E(B-V) < 0.15$, and the photometric redshift is $z_{\mathrm{phot}} = 8.3 \pm 0.3$, consistent with the spectroscopic results. We caution that the rest-frame wavelength observed extends only out to 2500Å, and only the three JHK filters do indeed measure any flux redwards of Lyman-α. That is the reason why the spectral index is only loosely constrained and its error is asymmetric ($\beta = 0.4^{+0.2}_{-1.4}$), although its relatively blue color still enables us to put stringent limits to the possible dust content in the afterglow environment. Supplementary Figure 4 shows the projections of the $(z, \alpha_O, \beta, E(B-V))$ four-dimensional confidence intervals on the different bidimensional planes.

Extending the analysis to the whole available temporal window ($2.5 \times 10^2 < t < 1.4 \times 10^6$ s) renders impossible to find a good fit with a single temporal power-law, because of the different decay regimes that the afterglow goes through.

3. Analysis of the TNG spectroscopic data

We observed the afterglow of GRB090423 with the near-IR camera and spectrograph NICS[40] on the Italian 3.6m Telescopio Nazionale Galileo (TNG) at La Palma. We used the the lowest spectral resolution mode, offered by the Amici prism[41]. This prism provides a simultaneous spectral coverage over a wide wavelength range, between 0.8 and 2.4 μm, and has a high efficiency. It yields a constant

spectral resolution $R \approx 50$ over the whole wavelength range. These characteristics make the instrument especially well-suited for studying the spectral distribution of faint objects.

We obtained 128 minutes of on-target spectroscopy. The afterglow was positioned in the slit using as reference a nearby star approximately 30 arcseconds away (at J2000 coordinates 09:55:35.31, +18:09:03.9). We used a dithering mosaic of 8 cycles, each including two coadds of single 120s exposures, repeated 4 times. The mean time of our observations was Apr 23.98, approximately 15.5 hours after the burst detection. The 2-dimensional spectrum is shown in Supplementary Figure 5.

Standard reduction tasks for NIR spectroscopy were performed independently by four different groups in our team, all of them reaching consistent results. Wavelength calibration was obtained by using a standard calibration table provided by the TNG and matching the deep telluric absorption bands. This method allows for wavelength calibrations better than 0.005 μm at 1.1 μm, and its contribution ($\Delta z = \pm 0.04$) to the final error budget on redshift is negligible.

Relative flux calibration was performed by using the observed spectral shape of the reference star. Its optical (SDSS) and near-IR (2MASS) colors are consistent with those of an M3-III star. The absolute calibration of the spectrum was obtained from the comparison with the simultaneous photometric measurements obtained by GROND (H=19.94 (Vega), ref. [7]). We estimate the slit losses to be less than 30%.

The observed flux is compatible with zero below a wavelength of 1.1 μm, while a significant flux ($> 99\%$ confidence level) is measured redwards of this limit. Assuming that this is due to hydrogen absorption by a virtually completely thick Lyman-α forest, then the redshift at which the GRB occurred is $z = 8.1^{+0.1}_{-0.3}$. The quoted error includes the uncertainties on the wavelength calibration and on the estimate of the break position. This value makes GRB090423 the most distant object spectroscopically identified to date. By using a standard cosmology with $\Omega_\Lambda = 0.73$, $\Omega_M = 0.27$, $H_0 = 71\,\mathrm{km s^{-1} Mpc^{-1}}$, we find that GRB 090423 was detected at a lookback time of greater than 13 Gyrs.

We tentatively identified two absorption features at 1.3 and 2.2 μm. These would be consistent with blends of Si IV and Fe II at 1400Å and 2400Å, $z = 8.1$ rest-frame, respectively. The detection, however, has a low confidence level due to the low S/N of the spectrum.

4. Modelling the GRB redshift distribution

We compute the probability of detecting of GRB 090423 in three different scenarios for the formation

and cosmic evolution of long GRBs: (i) no evolution model, where GRBs follow the cosmic star formation and their luminosity function (LF) is constant in redshift; (ii) luminosity evolution model, where GRBs follow the cosmic star formation but the LF varies with redshift; (iii) density evolution model, where GRBs form preferentially in low–metallicity environments. In the first two cases, the GRB formation rate is simply proportional to the global cosmic star formation rate as computed by [42]. For the luminosity evolution model, the typical burst luminosity is assumed to increase with redshift as $(1 + z)^\delta$. Finally, for the density evolution case, the GRB formation rate is obtained by convolving the observed SFR with the fraction of galaxies at redshift z with metallicity below Z_{th} using the expression computed by [43]. In this scenario, the LF is assumed to be constant.

The computation works as follows (see also [21,22,23,24,26,43]). The observed photon flux, P, in the energy band $E_{\min} < E < E_{\max}$, emitted by an isotropically radiating source at redshift z is

$$P = \frac{(1 + z) \int_{(1+z)E_{\min}}^{(1+z)E_{\max}} S(E)dE}{4\pi d_L^2(z)}, \tag{1}$$

where $S(E)$ is the differential rest–frame photon luminosity of the source, and $d_L(z)$ is the luminosity distance. To describe the typical burst spectrum we adopt the functional form proposed by [31], i.e. a broken power–law with a low–energy spectral index α, a high–energy spectral index β, and a break energy $E_b = (\alpha - \beta)E_p/(2 + \alpha)$, with $\alpha = -1$ and $\beta = -2.25$ (ref. [45]). In order to broadly estimate the peak energy of the spectrum, E_p, for a given isotropic–equivalent peak luminosity, $L = \int_{1\,\text{keV}}^{10000\,\text{keV}} ES(E)dE$, we assumed the validity of the correlation between E_p and L (ref. [46]).

Given a normalized GRB LF, $\phi(L)$, the observed rate of bursts with $P_1 < P < P_2$ is

$$\frac{dN}{dt}(P_1 < P < P_2) = \int_0^\infty dz \frac{dV(z)}{dz} \frac{\Delta\Omega_s}{4\pi} \frac{\Psi_{\text{GRB}}(z)}{1 + z} \int_{L(P_1,z)}^{L(P_2,z)} dL' \phi(L'), \tag{2}$$

where $dV(z)/dz$ is the comoving volume element, $\Delta\Omega_s$ is the solid angle covered on the sky by the survey, and the factor $(1 + z)^{-1}$ accounts for cosmological time dilation. $\Psi_{\text{GRB}}(z)$ is the comoving burst formation rate and the GRB LF is described by a power law with an exponential cut–off at low luminosities[47], i.e. $\phi(L) \propto (L/L_{\text{cut}})^{-\xi} \exp(-L_{\text{cut}}/L)$.

For the three scenarios, we optimize the model free parameters (GRB formation efficiency, burst typical luminosity at $z = 0$ and the power index ξ of the LF) by fitting the differential number counts observed by BATSE (see ref. [24,26] for a detailed description of the models and of the analysis). We

find that it is always possible to find a good agreement between models and data. Moreover, we can reproduce also the differential peak flux count distribution observed by Swift in the 15-150 keV band without changing the best fit parameters. On the basis of these results, we compute the probability to detect with Swift a GRB at $z \geq 8$ with photon flux P. The results are plotted in Supplementary Figure 6 (top panels) together with the cumulative number of GRBs at $z \geq 8$ expected to be detected by Swift in one year of observations (bottom panels). From the plot it is clear that the no evolution model fails to account for the observation of GRB 090423, since only $\sim 4 \times 10^{-4}$ GRBs are expected to be detected at $z \geq 8$ in ~ 4 years of Swift observations. Evolutionary models (both in luminosity or in density) can easily account for the discovery of GRB 090423. We note that the results confirm the need for cosmic evolution in the GRB luminosity function and/or in the GRB density obtained by recent analysis of the whole Swift GRB dataset. Indeed, both the large number of $z \geq 2.5$ bursts[24] and the number of bright (i.e. with peak luminosity $L \geq 10^{53}$ erg s^{-1}) bursts[26] strongly require the existence of evolution.

Moreover, we want to stress here that our conclusions are conservative. First of all, many biases can hampered the detection of GRB at very high redshift. Indeed, a few very high-z bursts may be hidden among the large sample of Swift bursts that lack of an optical detection. Thus, the discovery of a single event at $z > 8$ in 4.5 yrs of Swift operation can be treated as a lower limit on the real number of high-z detection. Moreover, our choice of the GRB LF is also conservative, since the existence of large population of faint GRBs (i.e. for an LF with a more gentle decline or a rise in the faint end) would lead to a decrease of the expecected number of GRBs at $z > 8$ strenghtening our conclusions.

31. Band, D.L. *et al.* BATSE observations of gamma-ray burst spectra. I - Spectral diversity. *Astrophys. J.* **413**, 281-292 (1993).

32. Zhang, B.-B. & Zhang, B. GRB 090423: pseudo burst at z=1 and its relation to GRB 080913. *GCN Circ.* 9216 (2009).

33. Amati, L. *et al.* On the consistency of peculiar GRBs 060218 and 060614 with the $E_{p,i} - E_{iso}$ correlation. *Astron. Astrophys.* **463**, 913-919 (2007).

34. Norris J.P. *et al.* Long-Lag, Wide-Pulse Gamma-Ray Bursts. *Astrophys. J.* **627**, 324-345 (2005).

35. Dickey, J.M. & Lockman F.J. H I in the Galaxy. *Annu. Rev. Astron. Astrophys.* **28**, 215-261 (1990).

36. Kalberla, P.M.W. *et al.* A New Whole HI Sky Survey. Proceedings of ASP Conference **317**, 13 (2004).

37. ev. sostituire con Campana in prep. Evans, P.A. *et al.* Methods and results of an automatic analysis of a complete sample of Swift-XRT observations of GRBs. ArXiv e-print:0812.3662 (2008).

38. Campana, S. *et al.* A Metal-rich Molecular Cloud Surrounds GRB 050904 at Redshift 6.3. *Astrophys. J. Lett.* **654**, 17-20 (2007).

39. Fernández-Soto A. *et al.* z-ph-REM: A photometric redshift code for the REM telescope. arXiv:astro-ph/0309492 (2003).

40. Baffa, C. *et al.* NICS: The TNG Near Infrared Camera Spectrometer. *Astron. Astrophys.* **378**, 722-728 (2001).

41. Oliva E. Infrared instrumentation for large telescopes : an alternative approach. MemSAIt **71**, 861 (2000)

42. Hopkins, A. M. & Beacom, J. F. On the Normalization of the Cosmic Star Formation History. *Astrophys. J.* **651**, 142-154 (2006).

43. Langer, L. & Norman, C. A. On the Collapsar Model of Long Gamma-Ray Bursts:Constraints from Cosmic Metallicity Evolution. *Astrophys. J. Lett.* **638**, 63-66 (2006).

44. Natarajan, P. *et al.* The redshift distribution of gamma-ray bursts revisited. *Mon. Not. R. Astron. Soc.* **364**, L8-L12 (2005).

45. Preece R. D. *et al.* The BATSE Gamma-Ray Burst Spectral Catalog. I. High Time Resolution Spectroscopy of Bright Bursts Using High Energy Resolution Data. *Astrophys. J. Suppl. Ser.* **136**, 19-36 (2000).

46. Yonetoku D. *et al.* Gamma-Ray Burst Formation Rate Inferred from the Spectral Peak Energy-Peak Luminosity Relation. *Astrophys. J.* **609**, 935-951 (2004).

47. Porciani, C. & Madau, P. On the Association of Gamma-Ray Bursts with Massive Stars: Implications for Number Counts and Lensing Statistics. *Astrophys. J.* **548**, 522-531 (2001).
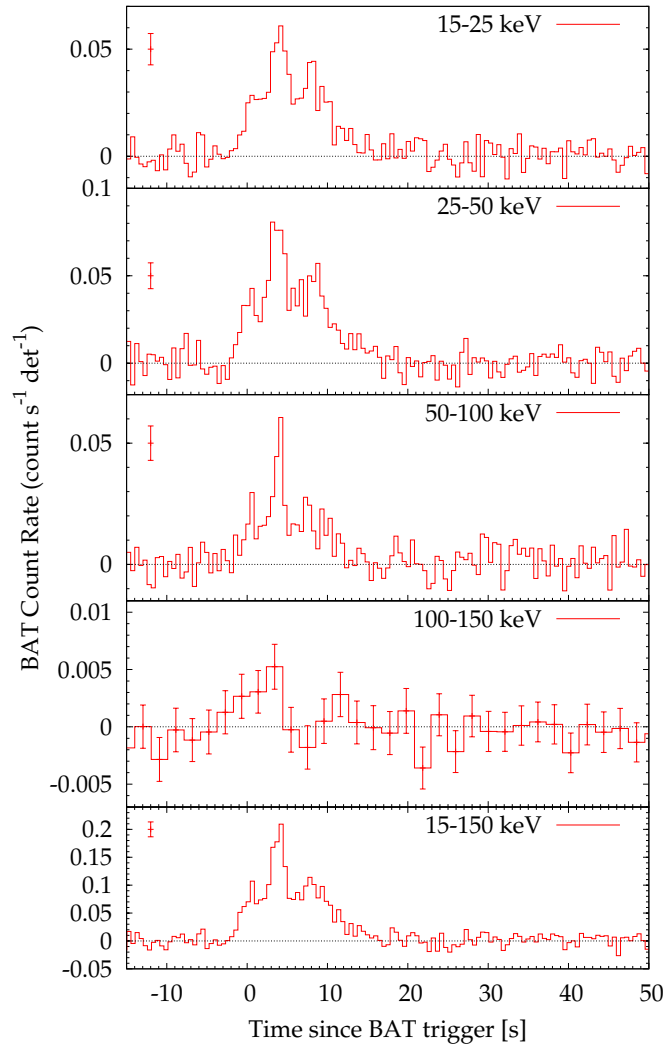
Supplementary Fig. 1. BAT mask-weighted light curve. Four channels and combined 0.512 s mask-weighted light curve. The light curve of the 100-150 keV energy channel shows a weak signal, because of the soft spectrum; the corresponding integration time is 2.048 s. Errors are at 1σ level.
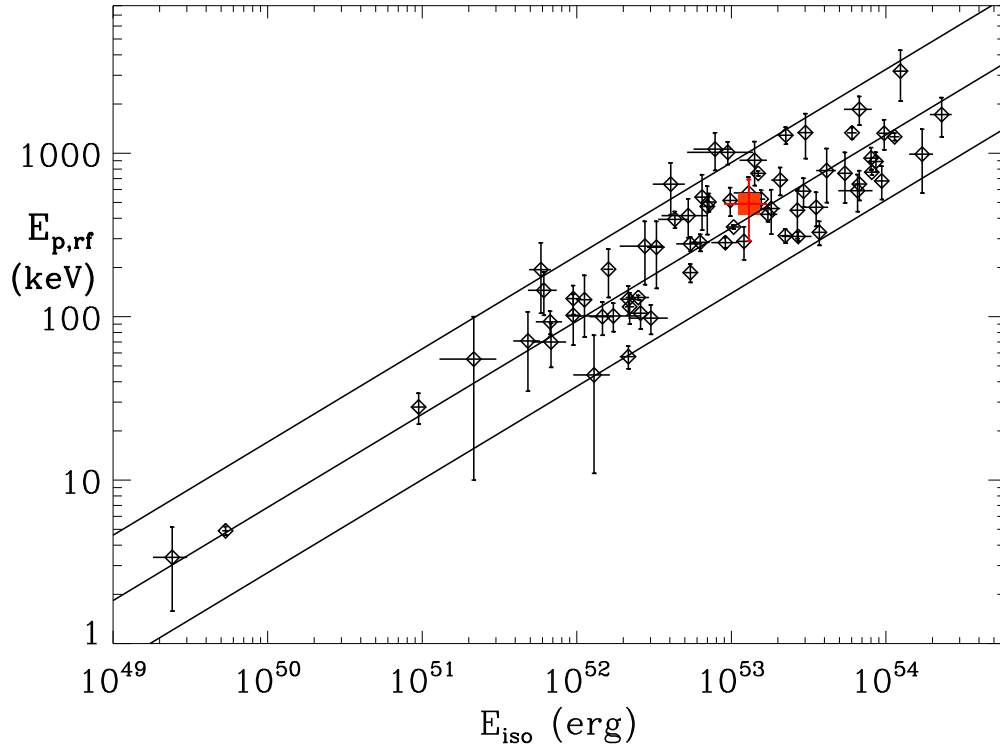
Supplementary Fig. 2. **Isotropic energy and peak energy correlation.** Position of GRB 090423 in the $E_{\rm p,rf}$ – E_{iso} plane based on Swift/BAT[4] and Fermi/GBM[10] (fitted with the Band function) results. The lines show the best–fit power–law and the $\pm 2\sigma$ region of the correlation as derived by [13]. Also shown are the 70 GRBs included in the sample analyzed in that work (errors on individual bursts are at 1σ level). Given that short GRBs do not follow the correlation[13], this evidence supports the hypothesis that, despite its cosmological rest–frame duration of ~ 1.3 s, GRB 090423 belongs to the long GRB class.
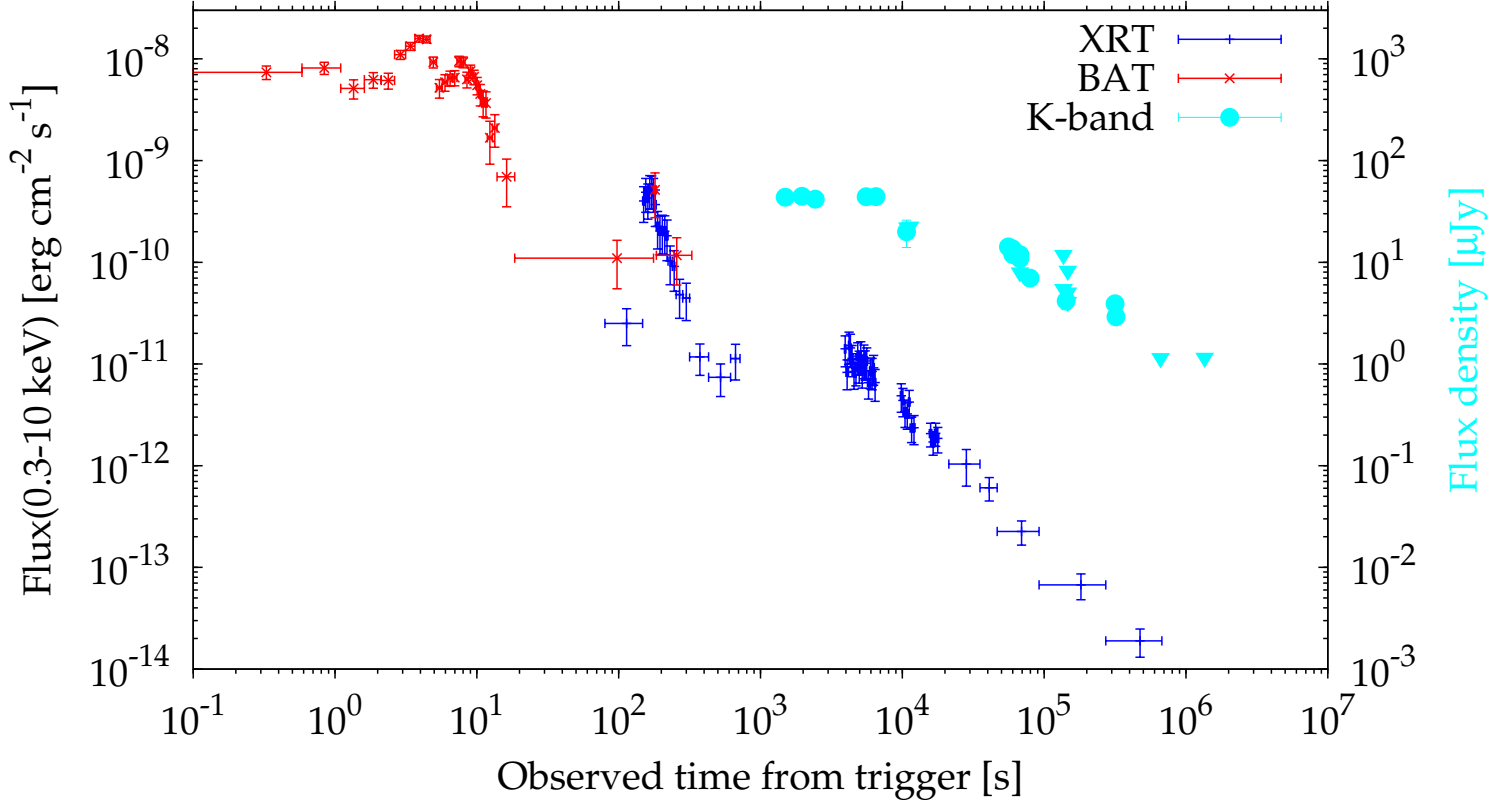
Supplementary Fig. 3. Observed light curve. Light curve of GRB 090423 as observed by Swift/BAT (red crosses), Swift/XRT (blue plus) and in the NIR (cyan points). Errors on fluxes are at 1σ level and horizontal bars refer to the integration time interval. The XRT 0.3–10 keV light-curve, starting at 73 s after the burst, shows a prominent flare at $t \sim 170$ s (also detected by BAT), and a flat phase ($\alpha_{X,1} = 0.13 \pm 0.11$) followed by a rather typical decay (starting at $t = 4513 \pm 491$ s) with power-law index $\alpha_{X,2} = 1.3 \pm 0.1$. Available photometric data are plotted in the K band (AB magnitude) by transforming the fluxes, when the observations have been taken in a different filter, using a power law with $\beta = 0.4$, as estimated from the NIR spectral energy distribution. A small displacement in time for contemporary data in different bands is applied in order to increase the visibility. The NIR light curve is consistent with a plateau phase ($t \sim 10^2 - 10^3$ s) followed by a decay with $\alpha_O \sim 0.5$ ($t \sim 10^3 - 10^5$ s). This decay phase is shallower than the X-ray decay in the same time interval. Triangles at $t \sim 10^5$ s report NIR upper limits as obtained by our second epoch TNG observation with the NICS camera in the Y and J band and by GROND in the JHK band. These limits are consistent with the temporal decay observed by XRT.
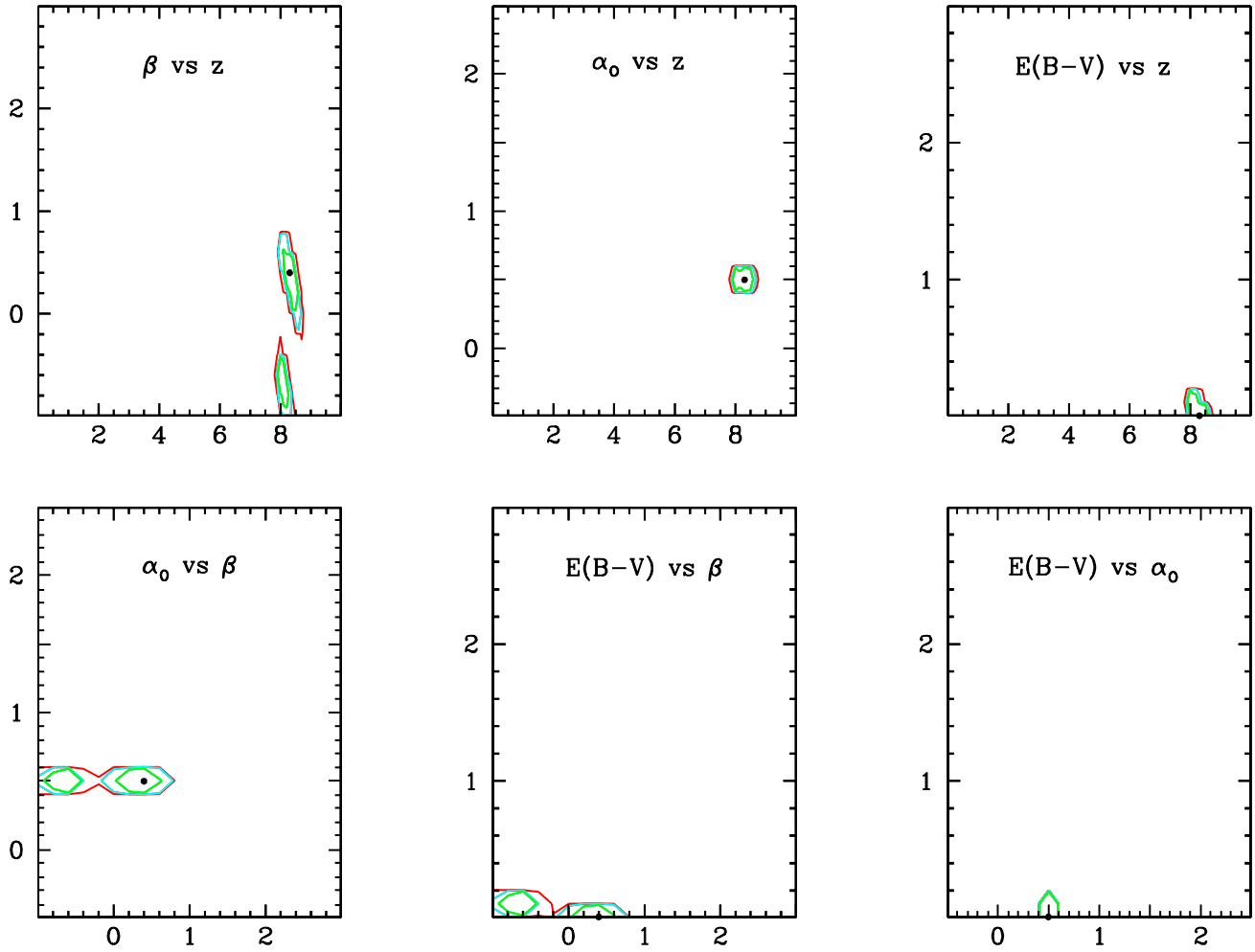
Supplementary Fig. 4. **Multi-parameter analysis of the photometric data.** Analysis of available photometric data for GRB090423 in the interval 70 min $< t <$ 1100 min. The code fits a model function with temporal index α_O and spectral index β, dust extinction $E(B-V)$, and redshift z. The different panels show the projection of the four-dimensional confidence intervals on the different two-dimensional planes of interest. The best-fit is marked by the black dot, with the red, cyan, and green contours defining respectively the 68%, 95%, and 99.5% confidence areas. The apparently bimodal distribution in the β direction is an artifact of the parameter space discretization.
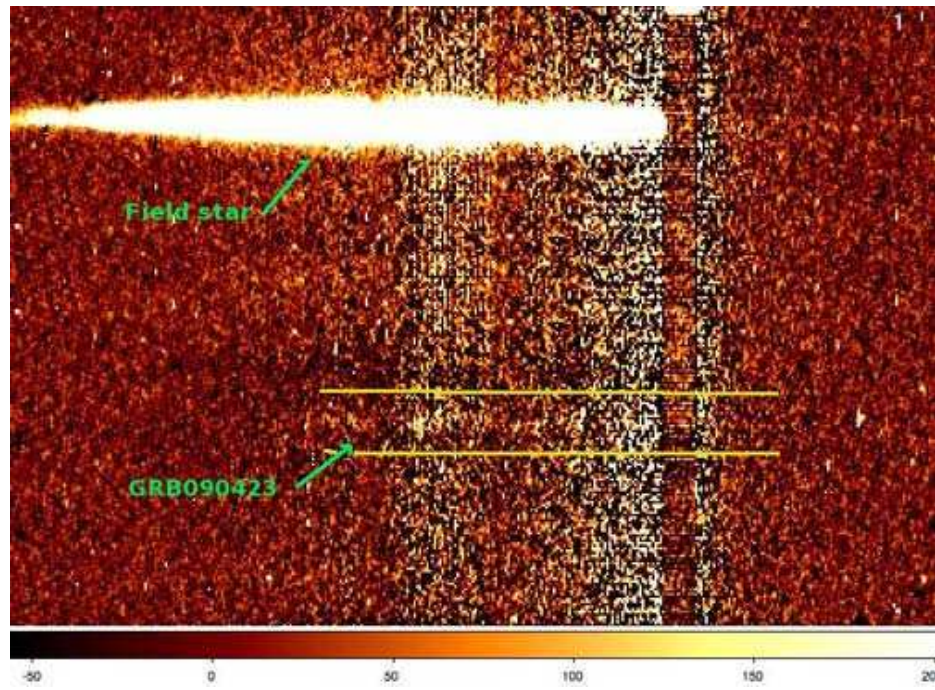
Supplementary Fig. 5.   **TNG 2-dimensional spectrum.** The spectrum has been taken by ~ 14 hrs from the trigger. The spectrum of the nearby reference star is also shown.
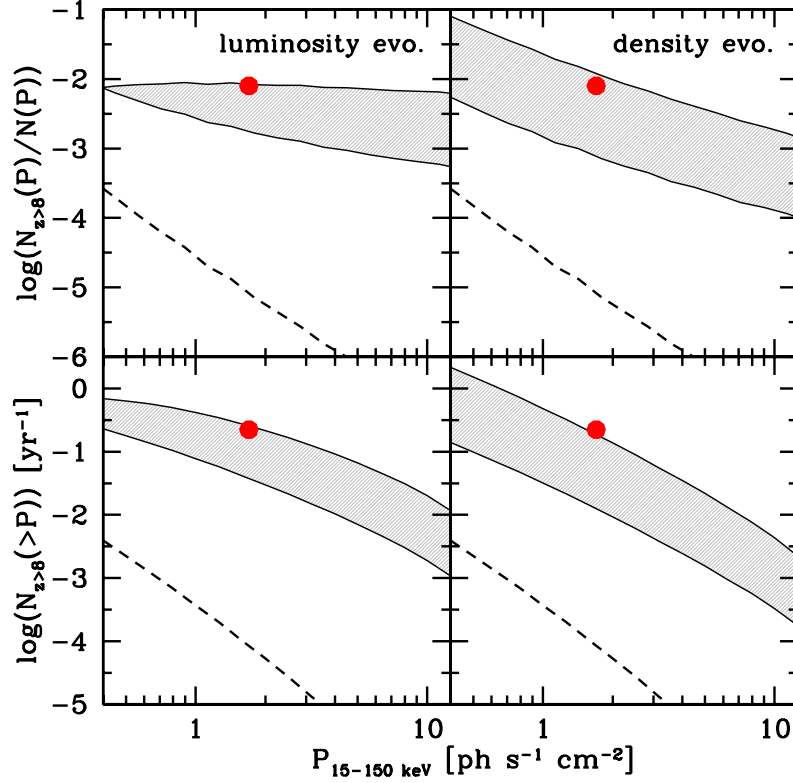
Supplementary Fig. 6. Probability of the occurance of GRB 090423. Top panels: probability for a GRB with peak photon flux P to be detected by Swift at $z \geq 8$. Luminosity evolution models are shown in the left panel, where shaded area refers to a typical burst luminosity increasing as $L_{\rm cut} \propto (1+z)^{\delta}$ with $\delta = 1.5 - 3$. Density evolution models are shown in the right panel, where shaded area refers to a metallicity threshold for GRB formation $Z_{th} = 0.02 - 0.2\, Z_{\odot}$ (the lower bound refers to the higher Z_{th}). In both panels, the dashed line shows the no evolution case. The red point marks the position of GRB 090423. We note that the point represents a lower limit on the number of detection at $z > 8$ since a few very high-z bursts may be hidden among those bursts that lack of an optical detection. Bottom panels: cumulative number of GRBs at $z > 8$ to be detected by Swift with photon flux larger than P in one year of Swift observations.